NeuroImage 251 (2022) 118985

Contents lists available at ScienceDirect

NeuroImage

journal homepage: www.elsevier.com/locate/neuroimage

Coherent theta oscillations in the cerebellum and supplementary motor area mediate visuomotor adaptation

Elinor Tzvi[a,*], Leila Gajiyeva[b], Laura Bindel[a], Gesa Hartwigsen[b], Joseph Classen[a]

[a] Department of Neurology, University of Leipzig, Liebigstraße 20, Leipzig 04103, Germany
[b] Lise Meitner Research Group Cognition and Plasticity, Max Planck Institute for Human Cognitive and Brain Sciences, Germany

A B S T R A C T

The cerebellum and its interaction with cortical areas play a key role in our ability to flexibly adapt a motor program in response to sensory input. Current knowledge about specific neural mechanisms underlying the process of visuomotor adaptation is however lacking. Using a novel placement of EEG electrodes to record electric activity from the cerebellum, we studied local cerebellar activity, as well as its coupling with neocortical activity to obtain direct neurophysiological markers of visuomotor adaptation in humans. We found increased theta (4–8 Hz) power in "cerebellar" as well as cortical electrodes, when subjects first encountered a visual manipulation. Theta power decreased as subjects adapted to the perturbation, and rebounded when the manipulation was suddenly removed. This effect was observed in two distinct locations: a cerebellar cluster and a central cluster, which were localized in left cerebellar crus I (lCB) and right supplementary motor area (rSMA) using linear constrained minimum variance beamforming. Importantly, we found that better adaptation was associated with increased theta power in left cerebellar electrodes and a right sensorimotor cortex electrode. Finally, increased rSMA -> lCB connectivity was significantly decreased with adaptation. These results demonstrate that: (1) cerebellar theta power is markedly modulated over the course of visuomotor adaptation and (2) theta oscillations could serve as a key mechanism for communication within a cortico-cerebellar loop.

1. Introduction

Adaptation to sudden environmental changes is at the root of basic human motor performance. For example, when walking on a moving train, our brain quickly produces an altered motor program using error-based learning mechanisms, that enables a steady and safe walking pattern. This process is referred to as sensorimotor adaptation. Previous behavioral studies in patients with cerebellar ataxia and cerebellar lesions due to stroke have demonstrated that the cerebellum plays a central role in this process (Criscimagna-Hemminger et al., 2010; Henriques et al., 2014; Schlerf et al., 2013; Tseng et al., 2007; Tzvi et al., 2021). Specifically, researchers hypothesized that sensory prediction errors, i.e. the difference between a predicted sensory outcome and the actual sensory feedback, is deficient in cerebellar patients, leading to worse performance in visuomotor adaptation tasks compared to healthy controls (Butcher et al., 2017; Henriques et al., 2014; Schlerf et al., 2013; Tseng et al., 2007; Wong et al., 2019). Others probed the role of the cerebellum in visuomotor adaptation using non-invasive electric stimulation, during or prior to task performance. Cerebellar direct current stimulation (tDCS) is thought to increase excitability in Purkinje cells, leading to inhibition of deep cerebellar nuclei and reduction of thalamic facilitation of cortical structures (Grimaldi et al., 2016). Cerebellar tDCS studies showed that stimulation of the cerebellar cortex led to enhanced visuomotor adaptation (Block and Celnik, 2013; Galea et al., 2011; Hardwick and Celnik, 2014; Weightman et al., 2020). Thus, enhanced visuomotor adaptation performance might be driven by increased excitability of Purkinje cells in the cerebellar cortex, leading to changes in connectivity with cortical areas, mediated by the inhibitory effect on the cerebello-dentato-thalamo-cortical pathway. Note, however, that replication attempts of this effect were not successful (Jalali et al., 2017; Liew et al., 2018; Mamlins et al., 2019), probably due to strong inter-subject variability in task performance as well as in response to the stimulation. Functional magnetic resonance imaging (MRI) studies may overcome this limitation by investigating network interactions that are individually associated with performance in the visuomotor adaptation task and thus account for inter-subject physiological differences. Indeed, these studies showed that the cerebellum and its interaction with cortical structures play an important role in visuomotor adaptation (Albert et al., 2009; Sami and Miall, 2013; Tzvi et al., 2020; Vahdat et al., 2011). Particularly, evidence suggests that cerebellar activity and connectivity is increased during resting-state following visuomotor adaptation (Albert et al., 2009; Sami and Miall, 2013; Vahdat et al., 2011), as well as dynamically with different phases of adaptation (Tzvi et al., 2020). However, as functional MRI relies on the BOLD signal which is an indirect measure of neuronal activity and connectivity, information regarding neuronal mechanisms of sensorimotor adaptation is still lacking.

The exact mechanism that allows flexible communication within a cortico-cerebellar network underlying visuomotor adaptation remains largely unknown. Communication within reverberating cortical-

* Corresponding author.
E-mail address: elinor.tzvi-minker@medizin.uni-leipzig.de (E. Tzvi).

https://doi.org/10.1016/j.neuroimage.2022.118985.
Received 21 October 2021; Received in revised form 25 January 2022; Accepted 7 February 2022
Available online 8 February 2022.

cerebellar loops is mainly mediated through deep cerebellar nuclei and the thalamus (Bostan et al., 2013; Nashef et al., 2018). To coordinate movement, the cerebellar cortex inhibits the deep cerebellar nuclei through Purkinje cells output, which are projected to the thalamus. The thalamus then exerts exciting influences on the motor and premotor cortices. "Communication through coherence" suggests though that oscillatory synchronization could serve as a marker for information transfer within neural networks (Fries, 2005). Accordingly, cerebellar oscillations may represent as key for communication within the cortical-cerebellar loop during visuomotor adaptation.

Testing this hypothesis in humans would require recordings of neuronal oscillations from the cerebellum. However, although oscillations from the cerebellum can relatively easily be recorded in animals using local field potentials (LFP) (D'Angelo et al., 2001), it has been debated whether non-invasive recordings are possible in humans using electroencephalography (EEG) or magnetoencephalography (MEG) (Andersen et al., 2020). A recent modeling study of EEG/MEG signals, combined with high-resolution MRI of an ex-vivo human cerebellum, has nonetheless found that cerebellar signals could indeed be reliably captured from the surface of the head (Samuelsson et al., 2020). Furthermore, both evoked and oscillatory cerebellar activity were found using MEG, in response to omissions of tactile stimuli (Andersen and Dalal, 2021). Additionally, EEG studies found that high-frequency cerebellar oscillations (Todd et al., 2018a) as well as vestibular cerebellar evoked potentials (Todd et al., 2018b), could be reliably detected in electrodes placed over the posterior fossa in humans. Finally, Pan and colleagues (2020) demonstrated that pathological cerebellar oscillations related to essential tremor could be recorded non-invasively in human patients. Importantly, these oscillations were validated by congruent LFP signals recorded from cerebellar cortex in the animal model. These findings testify to the feasibility of recording cerebellar oscillations in humans using EEG. Therefore, we hypothesized that direct insight in the physiology of sensorimotor adaptation in humans could be obtained by cerebellar EEG.

Previous cortical EEG studies investigated the underlying oscillatory pattern of visuomotor adaptation. Contreras-Vidal and Kerick (2004) found evidence for transient changes in theta (4–8 Hz), alpha (10–12 Hz) and low-beta (12–18 Hz) power, post movement, associated with early adaptation. The effect has then been replicated in several later studies in alpha (9–12 Hz) and beta (13–30 Hz) over sensorimotor areas (Fine et al., 2017; Tan et al., 2016) and parietal cortex (Savoie et al., 2018) as well as medial frontal areas (Fine et al., 2017), presumably associated with processes underlying visuomotor prediction errors as well as formation of motor memories. Whether similar patterns of oscillatory activity underlying visuomotor adaptation processes are evident in the cerebellum remains unknown.

In a recent fMRI study, we showed that cerebellar activity (along with other cortical structures), specifically increases as a response to a sudden exposure to a visuomotor rotation, decreases as visuomotor adaptation progresses, and increases again when the rotation is suddenly removed (Tzvi et al., 2020). In addition, directed connectivity analysis using Dynamic causal modeling revealed modulation of connectivity in the premotor-cerebellar loop by adaptation, such that interaction from cerebellum to premotor cortex was negatively modulated by adaptation, whereas interaction from premotor cortex to cerebellum was positively modulated by adaptation. Moreover, modulation of connection from cerebellum to premotor cortex was associated with a faster return to the original routine. Building on evidence from previous EEG studies and these prior fMRI results, we set out to investigate the specific neural mechanism that may underlie visuomotor adaptation changes in cerebellar activity and connectivity with cortical areas using EEG. In addition, we explored the effect of visuomotor adaptation on resting-state EEG data following the visuomotor adaptation task, as previous evidence from resting-state fMRI studies points to increased cerebellar activity and connectivity with cortical structures (Albert et al., 2009; Sami and Miall, 2013; Vahdat et al., 2011).

Specifically, we tested whether sensorimotor adaptation exhibits: (1) a unique pattern of cortical and cerebellar oscillations in theta (4–8 Hz), alpha (8–12 Hz) and beta (13–30 Hz) frequency bands and (2) coherent interactions between cerebellum and cortical structures. Our findings suggest that interactions within a cortico-cerebellar loop are mediated through coherent theta oscillations.

2. Materials and methods

2.1. Participants

26 healthy participants (mean age: 28 years, range 20–34; 7 males) took part in the experiment after giving informed consent. Participants were financially (10Euro/hour) compensated for their participation. All participants were classified as right-handed by means of the Edinburgh Handedness Inventory (Oldfield, 1971) (score: 84 ± 15) and had normal or corrected to normal vision. Participants were non-smokers and did not suffer from any mental or neurologic disorder (by self-report). We excluded professional musicians and computer gamers. One subject was excluded due to an error in the data acquisition and another subject due to lack of adaptation (see Section 2.1 below), resulting in a final sample of 24 subjects for the behavioral analysis. Two more subjects had to be excluded due to artifacts in the EEG signal and an error in electrode locations registration, resulting in a final cohort of 22 subjects for the EEG analyses. The study was approved by the Ethics Committee of the University of Leipzig (280/20-ek) and was performed in accordance with the Declaration of Helsinki.

2.2. Experimental paradigm and task design

During EEG recordings and task performance, subjects were seated comfortably in front of a 17″ computer screen, about 0.75 m away, on which visual stimuli were presented. The task was designed using Psychtoolbox-3 (Brainard, 1997) operating on MATLAB R2019b (Mathworks®). Prior to and following task performance, we recorded EEG during resting-state (RS), i.e., while subjects were focused on a cross in the center of the screen, for a duration of 200 s each. Subjects performed a visuomotor adaptation task, previously described by (Galea et al., 2011), with their right hand, using a digital pen moved on a digital tablet (Wacom Intuos Pro-L, Wacom, Kazo, Japan). The movements were visualized on the screen. A carton box covered the set-up to prevent visual feedback from the moving upper-limb. The position of the pen in 2D was sampled at 60 Hz, which means that adjacent sampling points had 17 ms between them. Subjects were instructed to perform straight, "shooting through" hand movements from a central starting point to a circular target in one of eight possible positions arrayed around a starting point at a distance of 70 mm, equally distributed every 45° (Fig. 1A). The targets were presented pseudo-randomly such that every set of eight consecutive trials included one of each target positions and thus each block of 24 trials included exactly 4 repetitions of each target. Trial description is presented in Fig. 1A. At the beginning of each trial, eight gray circles appeared around a center cross (i.e., the starting point) for 500 ms. Next, the target was marked as a blue circle and cued the subjects to start the movement towards the target. Note that this point in time was defined as stimulus onset for the EEG analyses described below. Movement onset was defined to be the first time point in which more than 20-pixel deviance between adjacent sampling points (~17 ms), in either direction, was detected. Once the pen crossed the invisible circle connecting the edges of all targets, all other stimuli disappeared and feedback was given as a green cross at movement end-point for 500 ms (Fig. 1A). This time point was defined to be movement cessation. The cursor was visible at all times. To encourage fast performance, a bar at the bottom of the screen indicated the elapsed time.

Over the course of the experiment, a 30° clockwise visuomotor perturbation of the cursor movement on the screen, was introduced abruptly (Fig. 1B). Subjects were not aware of this manipulation prior to

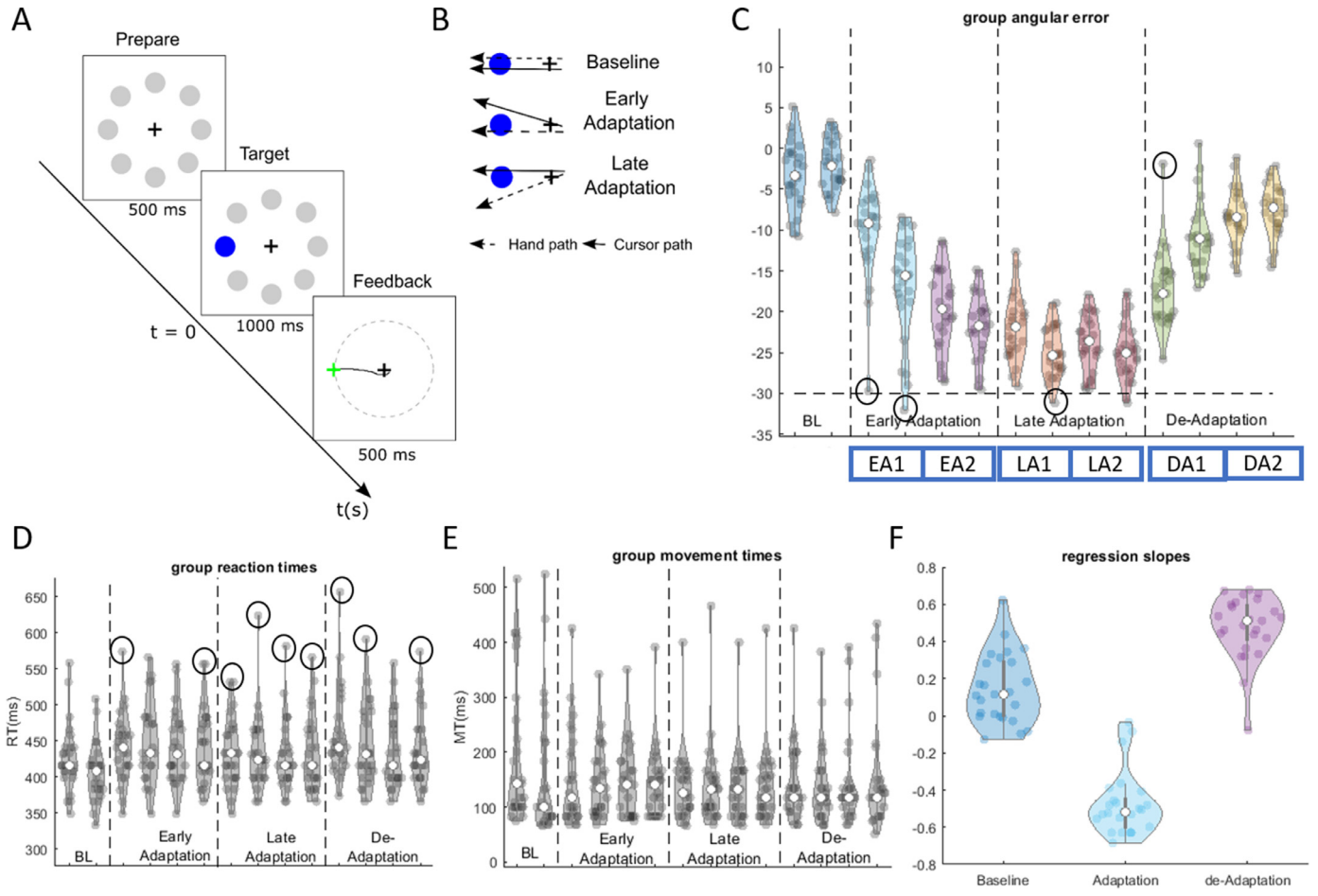

Fig. 1. Experimental design and behavioral results. **A** Trial timeline. Each trial began with 500 ms presentation of possible targets. Next, the current target was marked in blue, signaling the subjects to start the movement. This moment was defined as t = 0 ms for the EEG analyses to follow. When subjects crossed the imaginary circle connecting the edges of all targets, all other stimuli disappeared, and feedback was given using a green cross at the crossing point. **B** Task conditions and the corresponding hand and cursor paths. **C** Violin plots for the angular errors across subjects. With time and across adaptation blocks (EA1, EA2, LA1, LA2), subjects reach the optimal value of -30°, representing their adaptation to a 30° visual shift in the cursor path. When the perturbation is removed (DA1, DA2), subjects quickly re-adjust to the old routine. Black circles present values from the excluded subject. **D** Violin plots for reaction times across subjects, i.e., the time it took subjects to start the movement towards the target. Black circles present values from the excluded subject. **E** Violin plots for movement times across subjects, i.e., the interval between reaction time and the feedback. **F** Violinplots for linear regression slopes fitted for each subject.

the experiment. Later in the experiment, this perturbation was removed, also abruptly. The experiment was therefore divided into three phases: baseline (BL) containing simple center-target movements without perturbation, adaption (ADP) containing a 30° clockwise perturbation of the cursor movement on the screen, and de-adaptation (DA) phase in which the perturbation was removed. The experiment consisted of a total of 14 task blocks, each with 24 trials. In between the blocks 10 s breaks were introduced. Two blocks were included for the BL condition, the ADP and DA consisted of 8 and 4 blocks, respectively. The total task duration was ~20 min, depending on individual performance.

Prior to the main experiment, subjects performed a short familiarization with the task which consisted eight trials without perturbation as well as eight trials with random visual perturbations between 30° counter clockwise and 30° clockwise. In contrast to the main experiment, subjects could see their upper extremities during the familiarization phase. Following the main experiment, we asked the subjects whether they noticed a visuomotor perturbation and to describe it. Their answers were rated according to the extent of explicit knowledge of the manipulation as well as the use of a cognitive strategy in the experiment (0 – no knowledge, 6 – full knowledge). We used this behavioral parameter to investigate a possible association between awareness and oscillatory correlates of visuomotor adaptation.

2.3. Behavioral analysis

Analysis of behavioral data was performed using custom-made scripts in MATLAB. We assessed learning in each trial using the angular error, defined as the angle between a line connecting the center cross and the target, and a line connecting the center cross and the position of the cursor at peak velocity. A negative angular error describes movements performed counter clockwise during ADP to counter-act the 30° clockwise visual perturbation and successfully hit the target. A positive angular error describes movements performed clockwise. We excluded trials that had an angular error > 60° in any direction. To investigate the dynamics of single-trial angular errors in each condition (BL, ADP, DA), we fitted a linear regression curve to the angular errors across all trials (dependent variable: angular errors, independent variable: trial number) in conditions BL, ADP and DA, in each subject. Note that since the slope is highly susceptible to single-trial outliers, we only used this measure to estimate the direction of adaptation (see exemplary linear fits in supp. Fig. 1). The main behavioral measure of adaptation was the median angular error in each block (across 24 trials). The median was used since the data were not normally distributed.

Reaction times (RT) and movement times (MT) were also analyzed (Fig. 1D-E). RT was defined as the time difference between the appear-

ance of a target circle (circle color changes from gray to blue, Fig. 1A) and movement onset (defined above). MT was defined as the duration between movement onset and movement cessation. Outliers were excluded as described above. We calculated the median RT and MT in each block for each subject, again since the data were not normally distributed. We then analyzed differences in RT and MT between BL, ADP and DA using a Wilcoxon signed rank test (as the values were not normally distributed). Significance was set to $p < 0.05$.

2.4. MRI recordings

MRI images were recorded using a 3T Siemens Skyra or Siemens Prisma head-scanner with 32-channel head coil at the Max Planck Institute for Human Cognitive and Brain Sciences in Leipzig, Germany. A high resolution T1-weighted gradient-echo structural image was acquired using the following parameters: image matrix: 240 × 256, 176 sagittal slices of 1 mm thickness, TR = 2300 ms, TE = 2.98 ms.

2.5. EEG recordings

EEG was recorded in a non-shielded room using Ag/AgCl electrodes embedded in a custom 64-channel cap and connected to an eego™ amplifier (ANT Neuro b.v., Hengelo, the Netherlands) with a sampling-rate of 512 Hz and 24bit resolution. A low-pass filter was applied at 0.26*sampling-rate (~133 Hz) during acquisition. Electrodes were placed according to an extension of the 10–20 system at the following locations: Fp1, Fpz, Fp2, AFz (ground), F7, F5, F3, F1, Fz, F2, F4, F6, F8, FC5, FC3, FC1, FCz, FC2, FC4, FC6, T7, C5, C3, C1, Cz, C2, C4, C6, T8, TP7, CP5, CP3, CP1, CPz (online reference), CP2, CP4, CP6, TP8, P7, P5, P3, P1, Pz, P2, P4, P6, P8, PO7, PO5, PO3, POz, PO4, PO6, PO8, O1, Oz, O2, Iz. Six additional locations were recorded: CB11, CB1z, CB12, CB21, CB2z, CB22, located 5% inferior to Iz, and 10% laterally distributed over both left and right cerebellar hemispheres (yellow electrodes in Fig. 3A). Note that cerebellar locations as well as Iz were further than all other locations and therefor considered as a separate cluster for the EEG analysis below (see section 1.7). Electrode impedances were kept below 5kΩ.

2.6. EEG pre-processing

Pre-processing and all subsequent analyses were performed using in-house Matlab scripts, EEGLAB toolbox ver. 2021 (Delorme and Makeig, 2004) and Fieldtrip toolbox (Oostenveld et al., 2010). We first applied a high-order (5000 point) one-way finite-impulse response band-pass filter to remove slow drifts and power line noise. The filter had the following specifications: passband edges = 1–49 Hz, transition band-width: 0.33 Hz, cut-off frequencies at -6dB: 0.8 Hz, 49.2 Hz, no passband ripples and a stopband attenuation of -100 dB. Filtering was implemented using the EEGLAB function pop_eegfiltnew.m. Signals were then re-referenced offline to the average of the signal from left and right mastoids and the signal from electrode CPz was re-calculated. Then, signals were segmented into 3 s epochs, for task-based signals, -1 s to 2 s around stimulus onset. Note that a segmentation around movement onset was not possible due to technical reasons. An independent component analysis (ICA) procedure was then applied to the signals to identify components related to eye blinks and horizontal eye movements based on their topography and signal shape (Makeig et al., 2004). In most subjects, we removed 2–4 components. Additional epochs containing artifacts were removed using a simple threshold (-70μV, +70μV) on the filtered data (across subjects: <10% of all data).

2.7. Spectral power and statistical analysis

Next, we computed the power spectrum of the EEG signals using the Morlet wavelet. Signals were filtered to obtain oscillatory power using wavelets of seven cycle length. Frequency resolution was set to 2 Hz and time resolution to 50 ms. Task-based signals were then averaged across a 0–500 ms time window (T1, 0 ms being stimulus onset), which mostly accounts for motor preparatory signals but also movement initiation, and across a 500–1000 ms time window (T2), which accounts for both the movement and the feedback. Note that since the movement time was very short, it was not possible to disentangle these processes. Resting-state (RS) signals were averaged across the entire time window. Next and in order to limit the number of comparisons, we averaged the signals across the different frequency bands of interest: theta (4–8 Hz), alpha (9–13 Hz) and beta (14–30 Hz) shown to be modulated by visuomotor adaptation. In addition, and based on evidence from cerebellar EEG studies showing oscillations at higher frequency bands, we also explored whether visuomotor adaptation modulates oscillations in the gamma range (31–49 Hz). No correction was applied for the time prior to stimulus onset. To enhance statistical power and signal-to-noise ratio in task-based signals (Chen et al., 2021), we concatenated two blocks of 24 trials each for the EEG analysis, resulting in a total of 48 trials per block. This means that for the EEG analysis there was one block for BL, four blocks for ADP: two early adaptation blocks (EA1, EA2) and two late adaptation blocks (LA1, LA2) as well as two blocks for DA (DA1, DA2). Spectral power changes were assessed in the different time windows (T1: 0 - 500 ms, T2: 500 - 1000 ms), and across the different frequency bands (theta, alpha, beta and gamma).

To evaluate neural dynamics with adaptation, statistical tests were performed across subjects using 'ft_statfun_depsamplesFunivariate' (for rmANOVA) across the four ADP blocks (EA1, EA2, LA1, LA2). Post-hoc tests comparing different conditions, including BL and DA, at the different time windows, followed in order to obtain a more precise picture of oscillatory effects underlying visuomotor adaptation. In accordance with our hypothesis that cerebellar oscillations underlie visuomotor adaptation processes, we specifically focused the post-hoc tests on cerebellar electrodes. To examine changes in resting-state oscillatory activity following visuomotor adaptation, statistical tests were performed across subjects using 'ft_statfun_depsamplesT' comparing pre-task ("PRE") to post-task ("POST") resting-state EEG.

Both task-based and resting-state EEG analyses employed Monte Carlo permutation testing with 1000 randomizations. Clusters were specified using the Fieldtrip function 'ft_prepare_neighbours' as channel neighbors with a distance smaller than 40 mm. On average, for each channel, 4.1 neighboring channels were specified. As cerebellar channels and Iz were more than 40 mm away from the other electrodes, they were defined as a separate cluster without any neighbors. We report the cluster statistics as the sum of t-values for each electrode in the cluster, and the corrected p-value for the entire cluster. Significant differences between conditions were defined to encompass more than two electrodes with a p-level of 0.05 in a cluster. Post-hoc Wilcoxon signed-rank tests were performed across all electrodes in the identified cluster of the main analysis. P-values were corrected using the false discovery rate (FDR).

2.8. Source analysis

For source reconstruction, we used the linear constrained minimum variance (LCMV) beamforming approach. Following the pre-processing steps described above, signals were re-referenced to a common-average reference and band-passed filtered (Butterworth infinite impulse response, 4th order, zero phase forward and reverse, attenuation cut-off at -3dB: 4 - 8 Hz, no passband ripples, roll-off: -80 dB/decade) to extract theta (4 - 8 Hz) oscillations in T2 (500 – 1000 ms, stimulus onset: 0 ms), based on the findings from the electrode-space analysis (see Section 2.3 below). We then created a head model, specifying the individual head geometry based on T1 images of each subject (see specifications above), as well as tissue conduction properties, and applied the boundary element method (BEM) as a forward model. To this end, we segmented the T1 image into three tissue types: brain, skull and scalp and estimated for each tissue type (conductivities: 0.33, 0.004, 0.33 resp.) a boundary triangle mesh (brain: 3000 points, skull: 2000

points and scalp: 1000 points). We then aligned the individual electrode positions, recorded using Localite EEG PinPoint (Localite GmbH, Germany), to the head model. A source model, specifying the locations of sources within the head model was then constructed as a discrete grid based on the head model geometry. For each grid point, a lead field matrix was calculated, which was subsequently used to calculate the inverse spatial filter using LCMV. Source orientation was optimized by using the orientation of maximum signal power. To allow group level comparisons, individual source signals were then normalized using an MNI template. Statistical analyses of the source data were motivated by electrode-space results and in order to confirm the localization of effects. Specifically, we performed t-tests ('ft_statfun_desamplesT') using cluster-level Monte Carlo permutation testing, comparing the different task conditions (e.g., EA1 and BL) in accordance with the specific finding in the electrode-space analysis. Significant effects were defined based on a p-level of 0.05.

2.9. Connectivity analysis

To study causal interactions, i.e. the estimated direction of information flux between regions, we computed the phase-slope index (PSI, Nolte et al., 2008):

$$\widetilde{\Psi} = \sum_{f \in F} \left| C_{ij}(f) \right| \left| C_{ij}(f + \delta f) \right| \sin\left[\Phi(f + \delta f) - \Phi(f)\right]$$

Where, $C_{ij}(f) = S_{ij}(f)/\sqrt{S_{ii}(f)S_{jj}(f)}$ is the complex coherency, S is the cross-spectral matrix, δf is the frequency resolution, Φ is the phase spectrum and F is the set of frequencies over which the slope is summed. $\widetilde{\Psi}$ is then normalized by an estimate of the standard deviation: $\Psi = \widetilde{\Psi}/std(\widetilde{\Psi})$.

The PSI is a highly robust measure of connectivity between EEG signals which serves to estimate the direction of information flux. Thus, a positive PSI indicates that the signal from the first region is leading the signal from the second region and vice versa. To this end, we first computed the signals from the two identified ROIs in source space showing significant power changes with adaptation, namely: left cerebellar crus I (lCB) ROI and right supplementary motor area (rSMA) ROI (see Section 2.2 below). Then, we used the peak activity and individual spatial filters found in the source localization analysis described above. Next, spectral representations of the reconstructed signals were obtained using the fast Fourier transform (FFT) and multi-tapers (N = 5). Finally, we evaluated PSI using the Fieldtrip function 'ft_connectivity_psi' in each task condition (Bl, ADP, and DA) and block. Statistical analysis was performed using Wilcoxon signed-rank tests, comparing connectivity in EA1 to BL and EA1 to LA2, in accordance with the task-based analysis below (Section 2.2).

3. Results

3.1. Behavioral analysis

One subject was excluded from the behavioral analyses due to extreme small slopes in both adaptation (ADP) and de-adaptation (DA) blocks (-0.08, -0.08 resp., see supp. Fig. 1, P06) compared to the group's median (ADP: -0.52, DA: 0.51), as well as extreme slow reaction-times (ADP: 561 ms, DA: 582 ms) compared to the group's median (ADP: 416 ms, DA: 424 ms). Individual boxplots for the angular error in each block are presented in supp. Fig. 2. The distribution of explicit knowledge is presented in supp. Fig. 3. Most subjects (N = 16) were unaware of any manipulation (explicit score < 3). Three subjects were fully aware of the visuomotor perturbation. As this explicit recognition could have developed during the task, these subjects were not excluded from further analyses.

Violin plots for the group angular error in each block are presented in Fig. 1C. A linear regression curve was fitted for each subject for baseline (BL), ADP and DA. To test for dynamics in each task condition, we compared regression slopes to zero using a *t*-test. Regressions slopes in BL were in average positive (t_{23} = 4.3, p < 0.001), suggesting that subjects improved the negative angular errors during BL towards zero (see Fig. 1C & 1F). In ADP, regression slopes were in average negative (t_{23} = -15.9, p < e^{-13}) indicating adaptation to the visuomotor perturbation towards 30° Finally, in DA, slopes were again positive in average (t_{23} = 18.6, p < e^{-14}), indicating a rapid return to the original routine.

Reaction times analysis showed that subjects were slower in initiating movements to the visual target when the perturbation was introduced in the first block of ADP (compared to last block of BL, Z = 3.7, p < 0.001, Fig. 1D) as well as when the perturbation was removed in the first block of DA (compared to last block of ADP, Z = 3.1, p = 0.002, Fig. 1D). There were no differences between the first and the last block of ADP (p = 0.4). Movement times (Fig. 1E) did not differ between conditions and blocks (p > 0.1).

3.2. Neural oscillations evident during visuomotor adaptation

Next, we examined changes in cerebellar oscillatory power associated with visuomotor adaptation. To this end, we submitted power values in the different frequency bands (theta - θ, alpha - α, beta - β, gamma - γ), the two time-windows (T1: 0 - 500 ms, T2: 500 - 1000 ms) and across ADP blocks (EA1, EA2, LA1, LA2) to a rmANOVA and cluster-based Monte-carlo permutation analysis. Three different patterns of effects were observed (Fig. 2), suggesting differences in power values across ADP blocks. The first pattern (marked with an asterisk) was found in β, most evident in a frontal cluster during T1, as well as in α and β, most evident in a fronto-central cluster during T2 (clusterstat = 225.5. p = 0.002). The second pattern was found in cerebellar electrodes at θ and α during T1 and at θ during T2 (clusterstat = 108.4, p = 0.02). Finally, the third pattern (marked with an 'x') was found in T1 and T2 in θ over central electrodes (clusterstat = 85.5, p = 0.049). Note that one or two electrodes showing p-values lower than 0.05 were not considered as significant effects. However, as these effects were tested within the ADP condition only and across 4 consecutive blocks, they might be driven by changes in the oscillatory signal with time which are unrelated to adaptation per se. To better associate these oscillatory changes with visuomotor adaptation processes, we additionally compared the different adaptation phases to baseline (BL) and de-adaptation (DA).

3.3. Cerebellar oscillations underlying adaptation and de-adaptation

We first plotted time-frequency representations of exemplary cerebellar electrodes CB1z and CB2z (Fig. 3B), averaged across subjects at: (1) early adaptation compared to baseline (EA1-BL), (2) early adaptation compared to late adaptation (EA1-LA2) and (3) de-adaptation compared to the late adaptation (DA1-LA2). Increased θ power was evident across all the different comparisons, around 500–1000 ms (i.e., T2) following stimulus onset (appearance of the blue target circle), predominantly in electrode CB2z. Note that group reaction times were around 400–450 ms, suggesting that these effects on θ power occur during movement to the target and feedback, and correspond to previous findings from cortical EEG studies.

Based on these time-frequency representations of changes across adaptation phases, we followed the statistical analysis above with post-hoc cluster analysis in the different frequency bands and the different time windows separately. Specifically, we compared EA1 to BL to tap into oscillatory activity associated with the first exposure to the visual perturbation, as well as compared DA1 to LA2, i.e., when the perturbation was suddenly removed.

3.3.1. Effects in the theta frequency band

Indeed, we found significant condition differences most pronounced in cerebellar electrodes CB11, CB21, CB2z (p = 0.02, clusterstat = 6.8) and T2 time-window, showing increased θ power comparing EA1 to BL. There were no significant differences for T1. In source space (data not shown), we identified a peak activation in left cerebellum crus I (peak

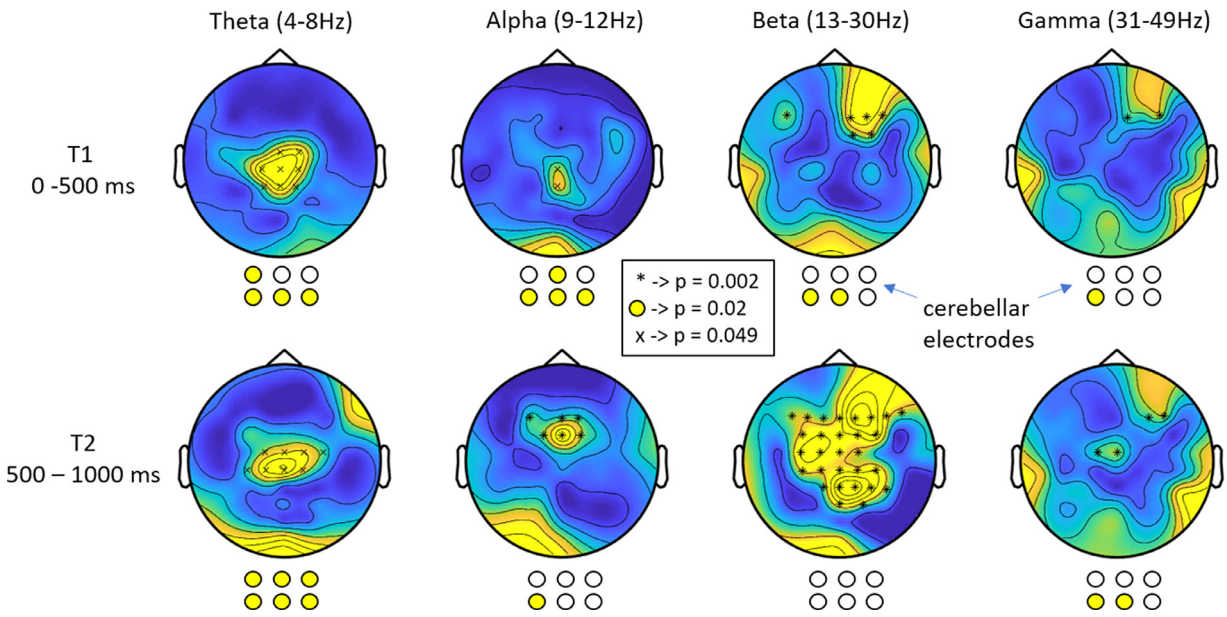

Fig. 2. Topographic plots for significant effects found across adaptation (EA1, EA2, LA1, LA2) in the different time windows (T1, T2) and the different frequency bands. Three different patterns were observed at different significance levels. The round circles represent the locations for cerebellar electrodes CB11, CB1z, CB12, CB21, CB2z, CB22 as shown in Fig. 3A.

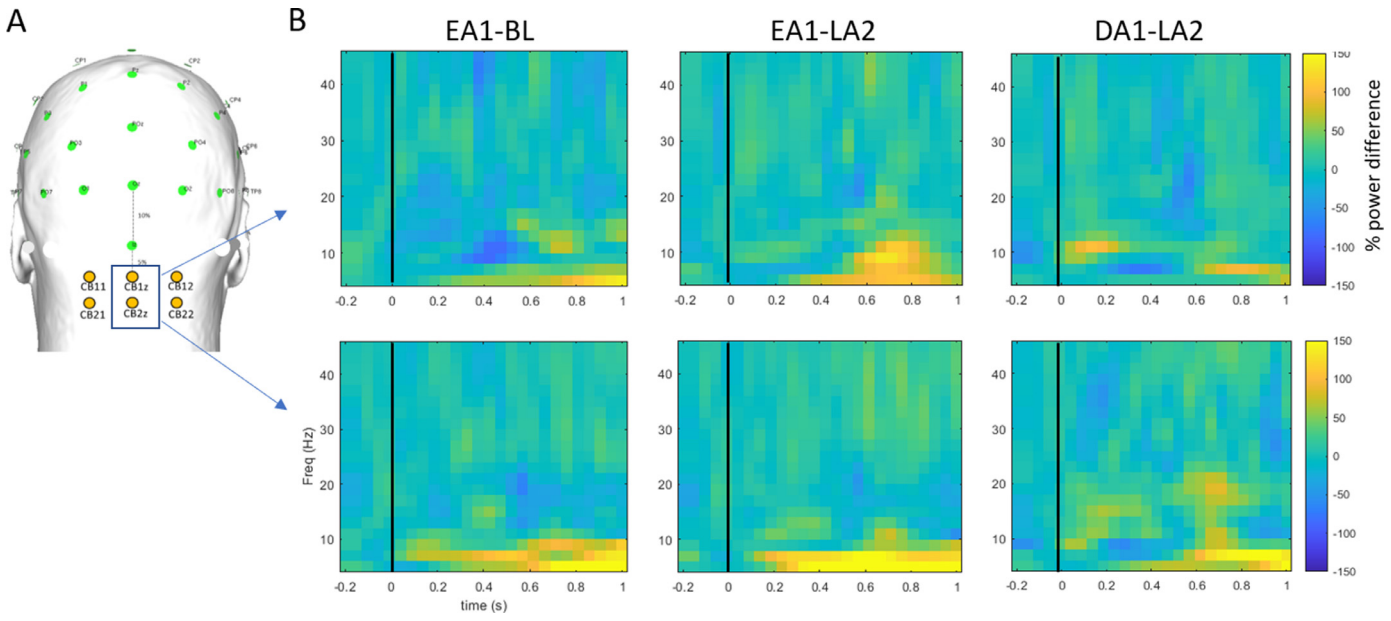

Fig. 3. **A** Locations of cerebellar electrodes (in yellow) on the surface of the head. **B** Time-frequency representations for locations CB1z and CB2z for three condition differences: early adaptation (EA1)-baseline (BL), early adaptation (EA1)-late adaptation (LA2), and de-adaptation (DA1)-late adaptation (LA2).

voxel: t_{21} = 3.1, p = 0.006), left inferior occipital lobe (peak voxel: t_{21} = 3.3, p = 0.002) as well as right cerebellar lobule VI (peak voxel: t_{21} = 3.1, p = 0.002) for the comparison between EA1 and BL.

θ power then decreased with adaptation in all cerebellar electrodes as revealed by post-hoc Wilcoxon signed-rank tests showing significant differences comparing EA1 to LA2 (all Z > 2.9, p < 0.004, FDR corrected, Fig. 4B). Reconstruction of this θ power changes in source space revealed peak activity in left cerebellar crus I (peak voxel: t_{21} = 3.3, p = 0.002, Fig. 4D) as well as left inferior occipital lobe (peak voxel: t_{21} = 3.7, p = 0.002, Fig. 4D). There were no significant activations in right cerebellum or right occipital cortex. Comparing DA1 to LA2, we found a trend for θ power increase in cerebellar electrode CB22 (Z = 2.1, p = 0.03, uncorrected). θ power was then significantly decreased from DA1 to DA2 in electrode CB22 (Z = 2.8, p = 0.005, FDR corrected). Here, source reconstruction revealed a small activation cluster in right cerebellum crus II (peak voxel: t_{21} = 4.1, p = 0.002, data not shown).

In order to demonstrate that these effects indeed reflect post-response and feedback processes, we performed post-hoc comparisons for θ power changes in all cerebellar electrodes, at pre- and post-response time windows, estimated from individual movement onsets (see full description of this analysis in supp. materials, Section 1). Thus, the resulting power changes reflect the individual changes associated with response and feedback processes. We found that these time-shifted θ power changes decreased with adaptation in all cerebellar electrodes (EA1 > LA2: all Z > 2.0, p < 0.016, FDR corrected), similarly to the stimulus-locked analysis above for T2. No significant effects were ob-

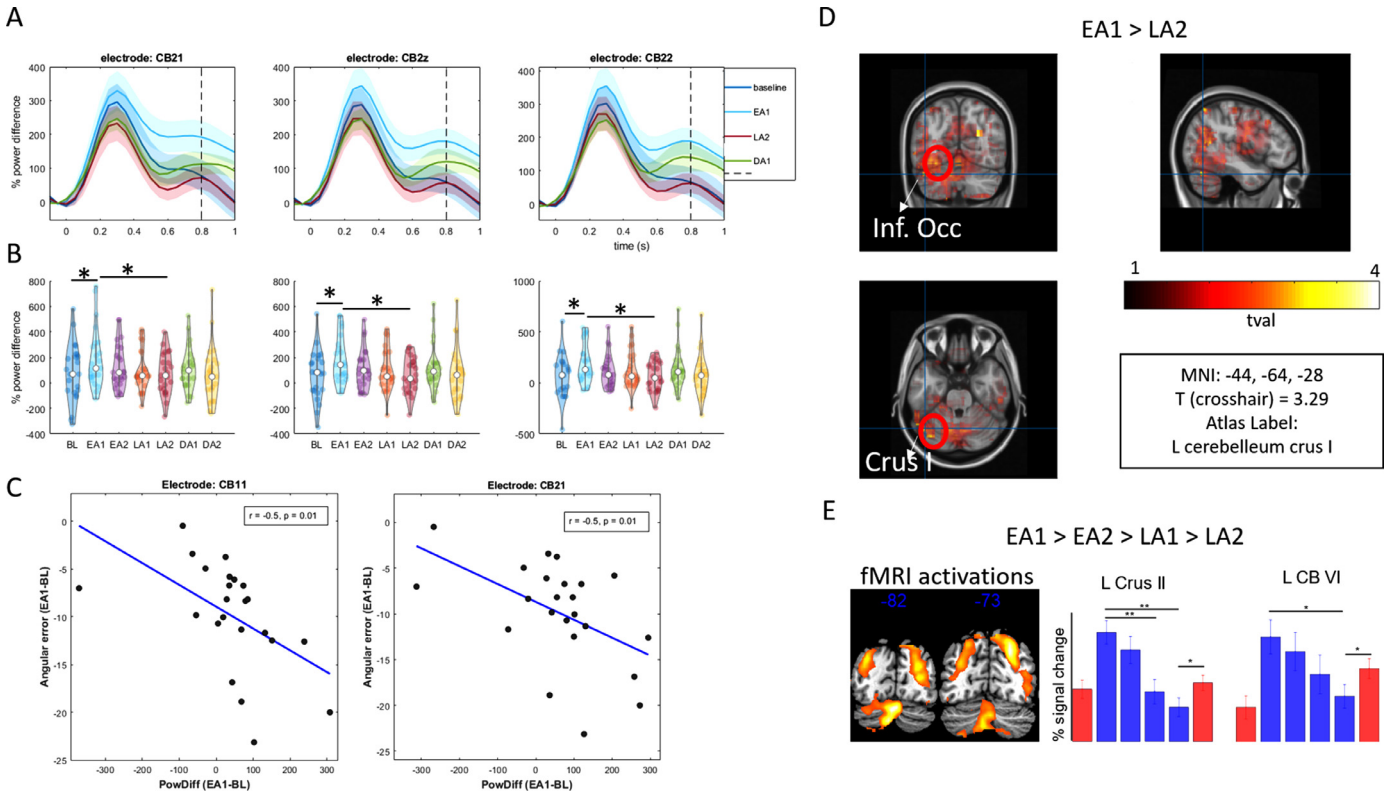

Fig. 4. **A** Theta oscillations in cerebellar electrodes across the different conditions. Specific for the T2 time window, theta power (% difference compared to pre-stimulus baseline) increased at early adaptation (EA1) compared to baseline (BL), attenuated as adaptation progressed, and rebounded at de-adaptation (DA1). Shaded areas are standard deviations of the mean across subjects. Dashed lines indicate the time point for which power values were extracted for B. **B** Violinplots for t = 0.8 s, at the peak of the T2 time window. Significant differences between conditions are marked with an asterisk for illustration. **C** Negative correlations between angular error and theta power difference in EA1-BL suggest that subjects that could better adapt early on, also exhibit larger theta power difference. **D** Source reconstruction for EA1-BL effects. **E** Activation patterns from previous fMRI study (Tzvi et al, Neuroimage 2020), showing differences from EA1 to LA2 and the corresponding pattern extracted from left cerebellar locations.

served for the other comparisons, nor for the pre-movement time window (see details in supp. materials, Section 1). Note that the estimation of movement onset is not as accurate compared to the stimulus onset, and might therefore obscure some of the effects observed above.

3.3.2. *Effects in the alpha frequency band*

In addition, we found significant α power increase in T2 (electrodes: CB21, CB22, p = 0.01, clusterstat = 4.7, data not shown) when comparing DA1 to LA2. However, α power did not change from EA1 to LA2 or between EA1 and BL (all p > 0.05), suggesting that these α power effects are not specific for adaptation. Analyses of T1 time-window and of β and γ power yielded non-significant effects using post-hoc tests (p > 0.05). We therefore focused the next analyses on θ power and T2 time-window.

3.3.3. *Theta power correlations with angular errors*

Next, we extracted EA1-BL θ power differences in T2 and electrodes CB11, CB21 and CB2z (showing significant EA1-BL power difference) and examined their association with differences in angular errors in EA1-BL. Here we focused on a specific time point in which maximal θ power was evident (t = 800 ms following stimulus onset, see Fig. 4B). We found a significant negative correlation between angular errors in EA1-BL and EA1-BL θ power differences at T2 in left cerebellar electrodes CB11 and CB21 (r = -0.52, -0.51 resp., p = 0.01, FDR corrected, Fig. 4C). This suggests that the observed θ power increase in EA1 was associated with stronger adaptation to the visuomotor rotation early-on. There were no correlations between power differences in other conditions and angular errors. There were no correlations between power differences and explicit awareness measures (all p > 0.1).

3.4. *Centro-parietal theta oscillations underlie visuomotor adaptation dynamics*

We recap the findings above. Power differences with adaptation were most pronounced in two cortical clusters: a centro-parietal θ cluster at T1 and T2 (clusterstat = 85.5, p = 0.049), and a frontal α cluster at T2, wide-spread β cluster at T2 and a right frontal β cluster at T1 (see Fig. 2). In accordance with our hypothesis above, we were specifically interested in effects spanning both cerebellar electrodes and cortical electrodes which may indicate communication within a cortical-cerebellar loop and therefore focused the following analyses on θ and T2 time window.

First, we found decreased θ power with adaptation, most pronounced in a central cluster (p = 0.01, clusterstat = 34.9, Fig. 5A-B). Post-hoc Wilcoxon signed-rank tests showed that θ power was significantly larger comparing EA1 to LA2 (all Z > 3.0, all p < 0.003, FDR corrected). Source reconstruction of this effect revealed a peak activity in right supplementary motor area (rSMA, peak voxel: t_{21} = 3.5, p = 0.002, Fig. 5C). θ power significantly increased from LA2 to DA1 in electrodes CP1, CP2, and CPz (all Z > 2.4, p < 0.02, FDR corrected). This θ power difference was associated with a source in right SMA (peak voxel: t_{21} = 3.3, p = 0.002). Similar to the analysis of response associated effects in cerebellar electrodes, here as well we tested whether time-shifted θ power, representing response and feedback processes (see supp. Materials Section 2 for further details), differs between adaptation conditions. Indeed, we found a significant increase in EA1 compared to BL in response-associated θ power in several electrodes of this cluster (see supp. Table 2). Electrodes CP1 and CP3 showed in addition a signifi-

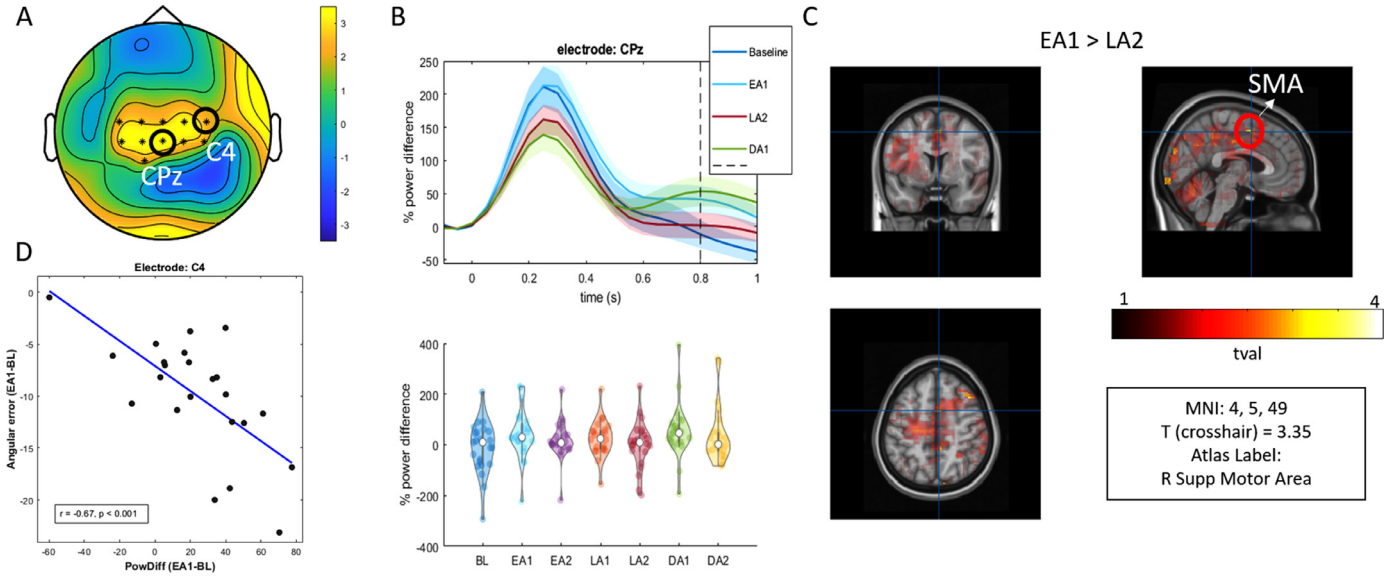

Fig. 5. **A** Topographic plot showing a cluster (locations marked with an asterisk) of significant theta power changes across adaptation. **B** Theta oscillations in electrode CPz. Shaded areas are standard deviations of the mean across subjects. Dashed line indicates the time point for which power values were extracted for the violinplot below. **C** Source reconstruction of EA1-LA2 theta power. **D** Negative correlation between theta power and angular errors in EA1-BL suggest that subjects that could better adapt early on, also exhibit larger theta power difference in C4.

cantly larger response-associated θ power comparing EA1 to LA2. No differences were observed between LA2 and DA1.

We next examined an association between EA1-BL θ power differences and EA1-BL differences in angular error, focusing on t = 800 ms following stimulus onset, similar to the analysis in cerebellar electrodes above. In electrode C4, we found a significant negative correlation ($r = -0.67$, $p < 0.001$, FDR corrected, Fig. 5D), suggesting that similar to the left cerebellar effects above, θ power increase in EA1 was associated with stronger adaptation to the visuomotor rotation early-on. There were no significant correlations between power differences in other conditions and behavior.

3.5. Modulation of resting-state oscillations by visuomotor adaptation

Next, we also analyzed possible changes in resting-state (RS) cerebellar oscillatory power following visuomotor adaptation, by examining the difference between pre-task RS (PRE) and post-task RS (POST) across the different frequency bands (θ, α, β, γ). We found increased θ power from PRE to POST specific for θ, in all cerebellar electrodes except CB12, (clusterstat = 13.19, p = 0.019, Fig. 6A). Across cortical locations using the same analysis in all other electrodes, we found a significant difference (clusterstat = 318, $p < 0.001$) showing increased θ but also α and β power (data not shown) from PRE to POST. A whole-brain source analysis for θ power revealed a significant effect in left cerebellar crus I ($t_{21} = 3.2$, p = 0.002, Fig. 6B), showing an increase from PRE to POST. There were no correlations between POST-PRE θ power in either cerebellar or cortical locations and the angular error differences EA1-BL ($p > 0.7$).

3.6. Modulation of cerebellar – SMA connectivity by visuomotor adaptation

To address the question whether interactions within the cortico-cerebellar loop are mediated by θ oscillations, we employed the phase-slope index (PSI) and studied directed changes in connectivity between left cerebellar crus I (lCB) and right SMA (rSMA) ROIs. The signals were extracted around the peak activation found above (see Fig. 4C and Fig. 5C). In addition, to control whether the effects are specific to the cerebellum and are not merely a reflection of occipital θ oscillations, we also analyzed connectivity between left occipital lobe (lOcc) and rSMA ROIs. Comparing EA1 to LA2, we found an increase in the directed interaction rSMA -> lCB (Z = 2.6, p = 0.009, FDR corrected, Fig. 7). No other differences between conditions were observed in rSMA -> lCB connectivity. Differences in directed connectivity lOcc -> rSMA between conditions were not significant ($p > 0.1$). There were no correlations between changes in angular error and rSMA -> lCB connectivity. Connectivity between lCB and rSMA during RS did not differ between PRE and POST ($p > 0.1$).

4. Discussion

In this study, we investigated oscillations as a neurophysiological marker for communication within visuomotor adaptation networks. We found evidence for changes in theta (θ, 4–8 Hz) power with adaptation to a visual perturbation in two main locations: a central-cluster and a cerebellar-cluster. In both clusters, θ power increased with first exposure to the perturbation, attenuated with time, and rebounded when the perturbation was removed. Modulation of θ power across different adaptation phases directly followed dynamic activation patterns observed in our previous fMRI study using the exact same task (Fig. 3D, Tzvi et al., 2020). Importantly, θ power differences were directly linked to changes in the angular error: subjects who better adapted to the visuomotor perturbation early-on, had larger θ power differences (compared to baseline) in electrodes placed over the left cerebellum (CB11, CB21) as well as electrode C4. Localization of θ power changes with adaptation using individual anatomical images suggested that sources for this effect reside in left cerebellar crus I (lCB) and right SMA (rSMA). Finally, we addressed the hypothesis that cortico-cerebellar interactions are mediated by θ oscillations by analyzing the phase-slope index (PSI) between rSMA and lCB during adaptation. We found increased rSMA->lCB interaction during early-adaptation compared to late adaptation, suggesting that θ oscillations underlie information transfer in the cortico-cerebellar network, essential for visuomotor adaptation processes.

Evidence for both low and high-frequency cerebellar oscillations is supported by previous recordings from cerebellar granule-cell layer in animals (for an overview see: De Zeeuw et al., 2008). In particular, low-frequency cerebellar oscillations (4–25 Hz) may serve to spatiotemporally organize communication through output to Purkinje cells as well as through synchronization between the cerebellum and cerebral cortex

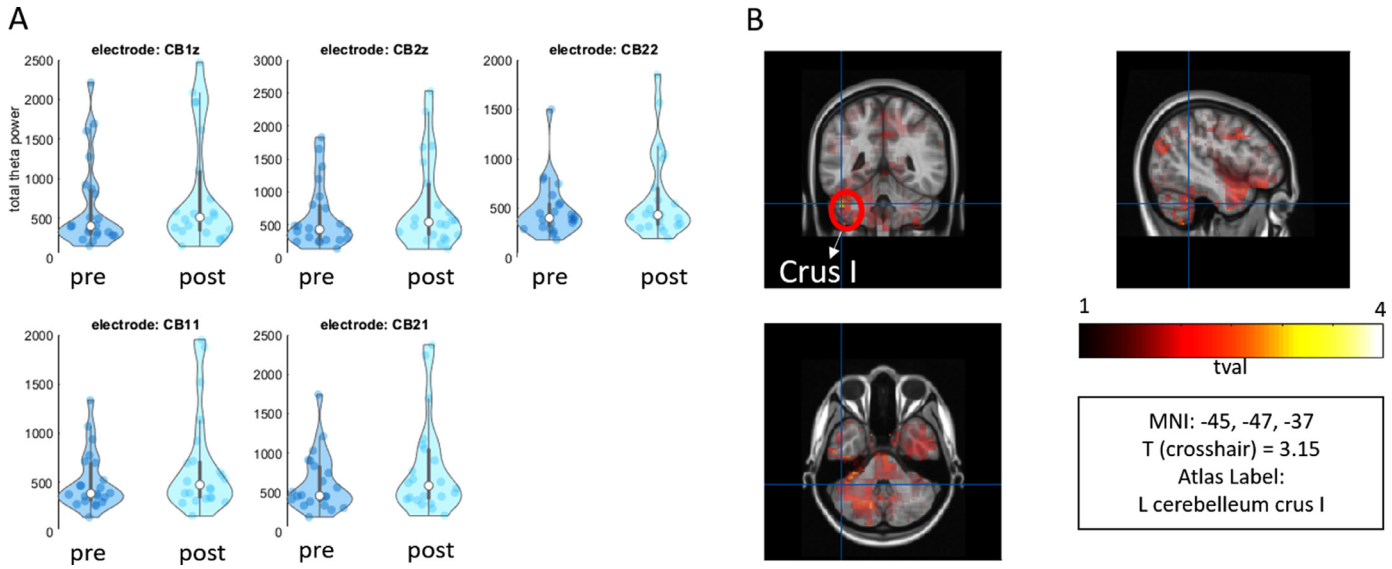

Fig. 6. Resting state theta oscillations. **A** Theta power increased from pre-task RS to post-task RS in electrodes over the cerebellum. **B** source analysis localized the effect to left cerebellar crus I.

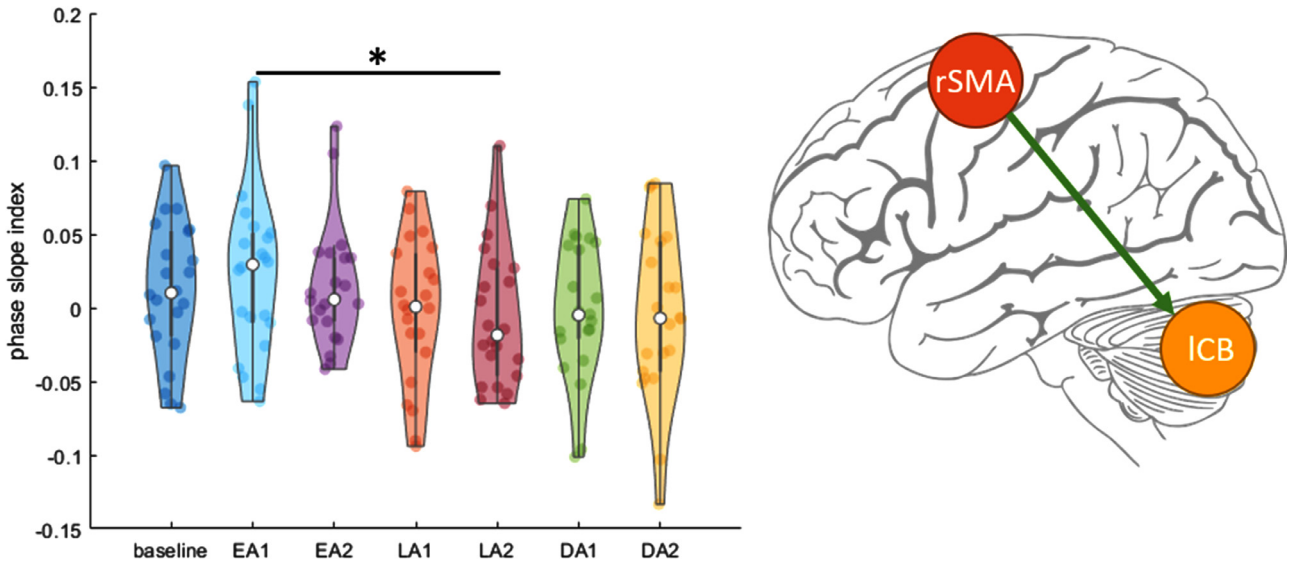

Fig. 7. Connectivity between left cerebellum crus I and right SMA. Early adaptation showed significantly stronger connectivity expressed as the phase-slope-index, compared to late adaptation.

(Courtemanche et al., 2013). Interestingly, LFP recordings from medial prefrontal cortex and cerebellum in guinea pigs showed increased synchronization in 5–12 Hz frequency band during eyeblink conditioning (Chen et al., 2016). Accordingly, these authors proposed that medial prefrontal cortex and cerebellar communication via θ-band synchronization contributes to adaptive associative learning behavior. Our results support and extend these findings, demonstrating interactions from right medial frontal cortex to left cerebellum during early visuomotor adaptation in humans. Note that while subjects performed the task with the right hand, the effects were mostly evident in left cerebellum and right SMA, i.e., contralaterally to the expected motor loop. This finding in left cerebellum coincides with our previous fMRI study, in which most activation associated with changes across adaptation were observed in the left cerebellum (Fig. 4E). Although, in that study we found interactions between left PMC and right cerebellum, we note that only left cortical nodes and right cerebellum were modelled for technical reasons. Therefore, we cannot exclude effects in right cortical and left cerebellum nodes. Importantly, it seems that cerebellar activity during visuomotor adaptation does not necessarily reflect pure motor activity along the cerebellar-motor loop but possibly a higher cognitive function.

Our findings further converge with previous EEG studies in humans. Using EEG source-localization, Mehrkanoon and colleagues (2016) showed increased functional connectivity in motor cortex-cerebellar interactions in oscillations around 10 Hz, during resting-state directly following training of a motor task. Importantly, they showed that the cerebellum phase-lags the motor cortex, which means that training of a motor task leads to enhanced directed information transfer from motor cortex to cerebellum. Notably this effect was also found in the left cerebellum (and left M1). The effect of visuomotor adaptation on cortical oscillations is also well studied with findings demonstrating effects in several frequency bands, including θ. For instance, Perfetti et al. (2011) found increased θ power in right posterior parietal scalp-region, for late relative to early adaptation, prior to movement initiation. This contrasts with current findings showing decreased θ power comparing late to early adaptation. We found no evidence to support modulation of θ power during movement

preparation but as our data analysis is rooted in effects locked to stimulus onset, we cannot exclude that the time window we selected for movement preparation contains movement. The previous study additionally reported that larger θ power during late adaptation (compared to early) was associated with a larger degree of adaptation (Perfetti et al., 2011). This converges with our observation that larger θ power in early adaptation (compared to baseline) is also associated with larger adaptation. Thus, it seems that increased θ power is indicative of successful adaptation, regardless of the specific adaptation phase. Finally, low θ (2–4 Hz, also referred to as delta) oscillations were found to be increased when visuomotor prediction errors, thought to reside in the cerebellum, were present (Savoie et al., 2018).

Interestingly, our findings of θ power modulation in the cerebellum are only in the posterior lobe, lobule VI, crus I and crus II. These are the most superficial sub-regions of the cerebellum and possibly the only regions from which cerebellar oscillations could be recorded (Samuelsson et al., 2020). Thus, it is impossible to assess whether the anterior cerebellum might also present with oscillatory activity underlying visuomotor adaptation.

To summarize, evidence suggests that θ oscillations may play an important role in the process of visuomotor adaptation, specifically as a mechanism for communication within a cortico-cerebellar network. Here, we found that not only cortical θ oscillations are relevant for visuomotor adaptation, but most importantly cerebellar θ oscillations. In accordance with the results by Mehrkanoon et al. (2016), we found increased directed θ coherence from rSMA to lCB during early adaptation, i.e. when prediction errors are large, compared to late adaptation when prediction errors were smaller.

Most commonly associated with learning and memory, vast empirical data suggest that θ oscillations are important for establishing temporal associations between sensory stimuli (for review see: Herweg et al., 2020). On the other hand, the cerebellum has been strongly associated with temporal representations of events, known as event timing (Ivry et al., 2002). Recently, it has been shown that the cerebello-thalamo-cortical pathway affects motor cortical firing at movement onset through synchronous bursts, which could serve as key for timing motor actions (Nashef et al., 2018). In our experiment, timely associations between proprioception and visual feedback develop as subjects adapt to the visual perturbation. Therefore, we speculate that increased cerebellar θ power reflects temporal integration of proprioception in the cerebellum (Bhanpuri et al., 2013) together with action programming in SMA. SMA might communicate the programmed action to the cerebellum when a mismatch between the action and the perception of the action on the screen occurs via a θ code, leading to increased θ connectivity during early adaptation.

The present results further converge with our previous fMRI study that investigated interactions within a cortico-striato-cerebellar network underlying visuomotor adaptation (Tzvi et al., 2020). Linear decrease in activity with adaptation was maximal in left cerebellum crus II as well as right SMA, corroborating the EEG findings here (again – despite being on the contralateral side, see above). Remarkably, θ power changes with adaptation followed the exact same activation pattern in the fMRI study: fMRI activity increased significantly when the perturbation was first introduced, decreased with adaptation and rebounded when the perturbation was removed during de-adaptation (Fig. 3D). These results suggest that the observed fMRI activation pattern likely reflect changes in θ power during visuomotor adaptation. Connectivity analysis using dynamic causal modeling revealed distinct modulation of interactions in a cerebellar-premotor cortex loop, such that connection from right cerebellum to left PMC was negatively modulated by adaptation but also the opposite connection from left PMC to right cerebellum was positively modulated by the adaptation process. Despite being evident on the contralateral premotor-cerebellar loop compared to the current results, it is likely that these interactions represent the same process taking place bilaterally as evident by the power analyses here and in our previous fMRI study (Tzvi et al., 2020). Note that both the premotor cortex as well as the SMA were evident in the fMRI analysis. Thus, the results of the current study not only replicate but also expand our previous fMRI findings in that they provide a possible mechanism in which communication with a cortico-cerebellar loop could take place. A future validation of this notion could be achieved for example using simultaneous EEG-fMRI recordings during performance in a visuomotor adaptation task.

Conclusions

In this study we demonstrate that cerebellar θ oscillations play a critical role in the process of visuomotor adaptation. Moreover, we propose that communication between cerebellum and SMA is mediated through coherent θ oscillations during the early adaptation phase, possibly for temporal integration of proprioception information in the cerebellum and a motor program in the SMA. These novel findings demonstrate that cerebellar oscillations could be detected using EEG and may motivate further investigation into cerebellar dynamics also in other domains.

Acknowledgments

The authors would like to thank Christoph Mühlberg and Anna Wolff for their assistance with the study design. In addition, we thank Orkan Ozcan (ANT Neuro / eemagine Medical Imaging Solutions GmbH) for his assistance with the EEG system and the “cerebellar cap” design. This study is supported by the German reseach foundation, grant TZ 85/1-1 to ET. We acknowledge support from the University of Leipzig for Open Access Publishing.

CRediT roles

ET: Conceptualization, Methodology, Software, Analysis, Writing, Funding acquisition, Project Administration. LG: Data collection, Data Curation. LB: Data collection, Methodology. GH: Writing, Project Administration, Supervision. JC: Writing, Supervision.

Data and code availability statement

The data and the code used in this study would be made available upon request.

Supplementary materials

Supplementary material associated with this article can be found, in the online version, at doi:10.1016/j.neuroimage.2022.118985.

References

Albert, N.B., Robertson, E.M., Miall, R.C., 2009. The resting human brain and motor learning. Curr. Biol. 19, 1023–1027. doi:10.1016/j.cub.2009.04.028.

Andersen, L.M., Dalal, S.S., 2021. The cerebellar clock: Predicting and timing somatosensory touch. Neuroimage doi:10.1016/j.neuroimage.2021.118202.

Andersen, L.M., Jerbi, K., Dalal, S.S., 2020. Can EEG and MEG detect signals from the human cerebellum? Neuroimage doi:10.1016/j.neuroimage.2020.116817.

Bhanpuri, N.H., Okamura, A.M., Bastian, A.J., 2013. Predictive modeling by the cerebellum improves proprioception. J. Neurosci. 33, 14301–14306. doi:10.1523/JNEUROSCI.0784-13.2013.

Block, H., Celnik, P., 2013. Stimulating the cerebellum affects visuomotor adaptation but not intermanual transfer of learning. Cerebellum 12, 781–793. doi:10.1007/s12311-013-0486-7.

Bostan, A.C., Dum, R.P., Strick, P.L., 2013. Cerebellar networks with the cerebral cortex and basal ganglia. Trends Cogn. Sci. doi:10.1016/j.tics.2013.03.003.

Brainard, D.H., 1997. The psychophysics toolbox. Spat. Vis. 10, 433–436. doi:10.1163/156856897X00357.

Butcher, P.A., Ivry, R.B., Kuo, S.H., Rydz, D., Krakauer, J.W., Taylor, J.A., 2017. The cerebellum does more than sensory prediction error-based learning in sensorimotor adaptation tasks. J. Neurophysiol. doi:10.1152/jn.00451.2017.

Chen, G., Pine, D.S., Brotman, M.A., Smith, A.R., Cox, R.W., Taylor, P.A., Haller, S.P., 2021. Hyperbolic trade-off: the importance of balancing trial and subject sample sizes in neuroimaging. Neuroimage 118786. doi:10.1016/J.NEUROIMAGE.2021.118786.

Chen, H., Wang, Y.J., Yang, L., Sui, J.F., Hu, Z.A., Hu, B., 2016. Theta synchronization between medial prefrontal cortex and cerebellum is associated with adaptive performance of associative learning behavior. Sci. Rep. doi:10.1038/srep20960.

Contreras-Vidal, J.L., Kerick, S.E., 2004. Independent component analysis of dynamic brain responses during visuomotor adaptation. Neuroimage 21, 936–945. doi:10.1016/J.NEUROIMAGE.2003.10.037.

Courtemanche, R., Robinson, J.C., Aponte, D.I., 2013. Linking oscillations in cerebellar circuits. Front. Neural Circ. doi:10.3389/fncir.2013.00125.

Criscimagna-Hemminger, S.E., Bastian, A.J., Shadmehr, R., 2010. Size of error affects cerebellar contributions to motor learning. J. Neurophysiol. 103, 2275–2284. doi:10.1152/jn.00822.2009.

D'Angelo, E., Nieus, T., Maffei, A., Armano, S., Rossi, P., Taglietti, V., Fontana, A., Naldi, G., 2001. Theta-frequency bursting and resonance in cerebellar granule cells: Experimental evidence and modeling of a slow K+-dependent mechanism. J. Neurosci. doi:10.1523/jneurosci.21-03-00759.2001.

De Zeeuw, C.I., Hoebeek, F.E., Schonewille, M., 2008. Causes and consequences of oscillations in the cerebellar cortex. Neuron doi:10.1016/j.neuron.2008.05.019.

Delorme, A., Makeig, S., 2004. EEGLAB: An open source toolbox for analysis of single-trial EEG dynamics including independent component analysis. J. Neurosci. Methods. doi:10.1016/j.jneumeth.2003.10.009.

Fine, J.M., Moore, D., Santello, M., 2017. Neural oscillations reflect latent learning states underlying dual-context sensorimotor adaptation. Neuroimage 163, 93–105. doi:10.1016/J.NEUROIMAGE.2017.09.026.

Fries, P., 2005. A mechanism for cognitive dynamics: neuronal communication through neuronal coherence. Trends Cogn. Sci. doi:10.1016/j.tics.2005.08.011.

Galea, J.M., Vazquez, A., Pasricha, N., Orban De Xivry, J.J., Celnik, P., 2011. Dissociating the roles of the cerebellum and motor cortex during adaptive learning: The motor cortex retains what the cerebellum learns. Cereb. Cortex 21, 1761–1770. doi:10.1093/cercor/bhq246.

Grimaldi, G., Argyropoulos, G.P., Bastian, A., Cortes, M., Davis, N.J., Edwards, D.J., Ferrucci, R., Fregni, F., Galea, J.M., Hamada, M., Manto, M., Miall, R.C., Morales-Quezada, L., Pope, P.A., Priori, A., Rothwell, J., Tomlinson, S.P., Celnik, P., 2016. Cerebellar transcranial direct current stimulation (ctDCS): a novel approach to understanding cerebellar function in health and disease. Neuroscientist doi:10.1177/1073858414559409.

Hardwick, R.M., Celnik, P.A., 2014. Cerebellar direct current stimulation enhances motor learning in older adults. Neurobiol. Aging doi:10.1016/j.neurobiolaging.2014.03.030.

Henriques, D.Y.P., Filippopulos, F., Straube, A., Eggert, T., 2014. The cerebellum is not necessary for visually driven recalibration of hand proprioception. Neuropsychologia doi:10.1016/j.neuropsychologia.2014.09.029.

Herweg, N.A., Solomon, E.A., Kahana, M.J., 2020. Theta oscillations in human memory. Trends Cogn. Sci. doi:10.1016/j.tics.2019.12.006.

Ivry, R.B., Spencer, R.M., Zelaznik, H.N., Diedrichsen, J., 2002. The Cerebellum and Event Timing. Annals of the New York Academy of Sciences doi:10.1111/j.1749-6632.2002.tb07576.x.

Jalali, R., Miall, R.C., Galea, J.M., 2017. No consistent effect of cerebellar transcranial direct current stimulation on visuomotor adaptation. J. Neurophysiol. doi:10.1152/jn.00896.2016.

Liew, S.L., Thompson, T., Ramirez, J., Butcher, P.A., Taylor, J.A., Celnik, P.A., 2018. Variable neural contributions to explicit and implicit learning during visuomotor adaptation. Front. Neurosci. doi:10.3389/fnins.2018.00610.

Makeig, S., Debener, S., Onton, J., Delorme, A., 2004. Mining event-related brain dynamics. Trends Cogn. Sci. doi:10.1016/j.tics.2004.03.008.

Mamlins, A., Hulst, T., Donchin, O., Timmann, D., Claassen, J., 2019. No effects of cerebellar transcranial direct current stimulation on force field and visuomotor reach adaptation in young and healthy subjects. J. Neurophysiol. doi:10.1152/jn.00352.2018.

Mehrkanoon, S., Boonstra, T.W., Breakspear, M., Hinder, M., Summers, J.J., 2016. Upregulation of cortico-cerebellar functional connectivity after motor learning. Neuroimage doi:10.1016/j.neuroimage.2015.12.052.

Nashef, A., Cohen, O., Israel, Z., Harel, R., Prut, Y., 2018. Cerebellar shaping of motor cortical firing is correlated with timing of motor actions. Cell Rep doi:10.1016/j.celrep.2018.04.035.

Nolte, G., Ziehe, A., Nikulin, V.V., Schlögl, A., Krämer, N., Brismar, T., Müller, K.R., 2008. Robustly estimating the flow direction of information in complex physical systems. Phys. Rev. Lett. doi:10.1103/PhysRevLett.100.234101.

Oldfield, R.C., 1971. The assessment and analysis of handedness: the Edinburgh inventory. Neuropsychologia doi:10.1016/0028-3932(71)90067-4.

Oostenveld, R., Fries, P., Maris, E., Schoffelen, J.-M., Oostenveld, R., Fries, P., Maris, E., Schoffelen, J.-M., 2010. FieldTrip: open source software for advanced analysis of MEG, EEG, and invasive electrophysiological data, FieldTrip: open source software for advanced analysis of MEG, EEG, and invasive electrophysiological data. Comput. Intell. Neurosci. Comput. Intell. Neurosci. 2011. doi:10.1155/2011/156869, 2011, e156869.

Pan, M.K., Li, Y.S., Wong, S.B., Ni, C.L., Wang, Y.M., Liu, W.C., Lu, L.Y., Lee, J.C., Cortes, E.P., Vonsattel, J.P.G., Sun, Q., Louis, E.D., Faust, P.L., Kuo, S.H., 2020. Cerebellar oscillations driven by synaptic pruning deficits of cerebellar climbing fibers contribute to tremor pathophysiology. Sci. Transl. Med. doi:10.1126/scitranslmed.aay1769.

Perfetti, B., Moisello, C., Landsness, E.C., Kvint, S., Lanzafame, S., Onofrj, M., Di Rocco, A., Tononi, G., Ghilardi, M.F., 2011. Modulation of gamma and theta spectral amplitude and phase synchronization is associated with the development of visuo-motor learning. J. Neurosci. doi:10.1523/JNEUROSCI.1319-11.2011.

Sami, S., Miall, R.C., 2013. Graph network analysis of immediate motor-learning induced changes in resting state BOLD. Front. Hum. Neurosci. 7. doi:10.3389/fnhum.2013.00166.

Samuelsson, J.G., Sundaram, P., Khan, S., Sereno, M.I., Hämäläinen, M.S., 2020. Detectability of cerebellar activity with magnetoencephalography and electroencephalography. Hum. Brain Mapp. doi:10.1002/hbm.24951.

Savoie, F.A., Thénault, F., Whittingstall, K., Bernier, P.M., 2018. Visuomotor prediction errors modulate EEG activity over parietal cortex. Sci. Rep. doi:10.1038/s41598-018-30609-0.

Schlerf, J.E., Xu, J., Klemfuss, N.M., Griffiths, T.L., Ivry, R.B., 2013. Individuals with cerebellar degeneration show similar adaptation deficits with large and small visuomotor errors. J. Neurophysiol. 109, 1164–1173. doi:10.1152/jn.00654.2011.

Tan, H., Wade, C., Brown, P., 2016. Post-movement beta activity in sensorimotor cortex indexes confidence in the estimations from internal models. J. Neurosci. doi:10.1523/JNEUROSCI.3204-15.2016.

Todd, N.P.M., Govender, S., Colebatch, J.G., 2018a. The human electrocerebellogram (ECeG) recorded non-invasively using scalp electrodes. Neurosci. Lett. doi:10.1016/j.neulet.2018.06.012.

Todd, N.P.M., Govender, S., Colebatch, J.G., 2018b. Vestibular cerebellar evoked potentials in humans and their modulation during optokinetic stimulation. J. Neurophysiol. doi:10.1152/jn.00502.2018.

Tseng, Y.W., Diedrichsen, J., Krakauer, J.W., Shadmehr, R., Bastian, A.J., 2007. Sensory prediction errors drive cerebellum-dependent adaptation of reaching. J. Neurophysiol. doi:10.1152/jn.00266.2007.

Tzvi, E., Koeth, F., Karabanov, A.N., Siebner, H.R., Krämer, U.M., 2020. Cerebellar – Premotor cortex interactions underlying visuomotor adaptation. Neuroimage doi:10.1016/j.neuroimage.2020.117142.

Tzvi, E., Loens, S., Donchin, O., 2021. Mini-review: the role of the cerebellum in visuomotor adaptation. Cerebellum doi:10.1007/s12311-021-01281-4.

Vahdat, S., Darainy, M., Milner, T.E., Ostry, D.J., 2011. Functionally specific changes in resting-state sensorimotor networks after motor learning. J. Neurosci. doi:10.1523/JNEUROSCI.2737-11.2011.

Weightman, M., Brittain, J.S., Punt, D., Miall, R.C., Jenkinson, N., 2020. Targeted tDCS selectively improves motor adaptation with the proximal and distal upper limb. Brain Stimul doi:10.1016/j.brs.2020.02.013.

Wong, A.L., Marvel, C.L., Taylor, J.A., Krakauer, J.W., 2019. Can patients with cerebellar disease switch learning mechanisms to reduce their adaptation deficits? Brain doi:10.1093/brain/awy334.